Asian Journal of Chemistry; Vol. 26, No. 18 (2014), 6089-6096

ASIAN JOURNAL OF CHEMISTRY

http://dx.doi.org/10.14233/ajchem.2014.16716

Photocatalytic Degradation Mechanism of Reactive Brilliant Blue X-BR by Expanded Perlite/TiO_2

XI QUAN WANG*, SHI YING FAN and YI NAN WANG

Department of Environmental Engineering, School of Chemical Engineering, Liaoning University of Science and Technology, Anshan 114051, P.R. China

*Corresponding author: Tel: +86 18941222346; E-mail: wxq_as@163.com

Received: 19 November 2013; *Accepted*: 21 March 2014; *Published online*: 1 September 2014; AJC-15860

Expanded perlite loaded titanium dioxide photocatalysts were prepared by a sol-gel method. Expanded perlites were modified using H_2SO_4 and cetyltrimethylammonium bromide in this experiment. The photocatalytic degradation mechanism of Reactive brilliant blue X-BR by expanded perlites loaded titanium dioxide photocatalysts has been investigated. The samples were characterized by scanning electron microscopy, specific surface area, X-ray diffraction analysis. The photocatalytic activities were evaluated by the photocatalytic oxidation of Reactive brilliant blue X-BR solution. It was found that the prepared expanded perlite loaded titanium dioxide photocatalysts have an excellent photocatalytic under ultraviolet illumination. The results of ultraviolet spectrum and infrared absorption spectrum showed that the anthraquinone structures and benzene rings were destroyed under photocatalytic oxidation reaction. The identification by gas chromatography-mass spectrometer analyses indicated that H_2O and carbon dioxide could be the primary degradation products.

Keywords: Photocatalytic degradation mechanism, Reactive brilliant blue X-BR, TiO_2, Expanded perlites.

INTRODUCTION

Anthraquinone dyes are difficult to biodegradation by their aromatic structures and azo-based ones. Anthraquinone reactive dyes have gradually attracted critical attention from the toxicological and environmental points of view, particularly in light of the current increase in their applications[1]. Recent reviews[2] indicated that titanium dioxide (TiO_2) has been widely used because it is easily available, inexpensive, non-toxic and shows relatively a high chemical stability. Titanium dioxide photocatalyst is very promising for application to water purification, because many hazardous organic compounds can be decomposed and mineralized by the proceeding oxidation and reduction processes on the TiO_2 surface[3]. Because of the particle density of TiO_2 is greater than water, it can hardly to be recycled, so finding the perfect carrier becomes very significant. Hollow glass beads[4], sepiolites[5] and montmorillonites[6] have been utilized as carriers. Expanded perlite (EP) was made an excellent alternative because of its characteristics, such as light qualitative, porous, small thermal conductivity, high chemical stability, low price, big surface area and strong adsorption ability[7], leading to an increase in the recycle rate of the photocatalysts. Consequently, expanded perlite loaded TiO_2 (EP/TiO_2) is considered a promising photocatalyst with an industrial application.

Degradation mechanism could not only provide reliably experiment theoretical basis for actual wastewater treatment, but can also improve the efficiency of wastewater treatment and reduce blindness. Earlier work has demonstrated that the reaction rate of H_2SO_4 and cetyltrimethylammonium bromide modified expanded perlite (HCEP) was best, we made an attempt to investigate the intermediate products and degradation pathways of Reactive brilliant blue X-BR(X-BR) solution with photocatalytic oxidation. The structural transformation of X-BR were identified through ultraviolet spectrum, infrared absorption spectrum and gas chromatography-mass analysis.

EXPERIMENTAL

The anthraquinone reactive brilliant blue X-BR (technical pure) was purchased from Shanghai Hufeng biochemical reagents Co. LTD. Before the photocatalytic oxidation experiments, the Reactive brilliant blue X-BR dye stock solution (1000 mg/L) was prepared and then diluted to 50 mg/L with deionized water. The initial pH of the diluted Reactive brilliant blue X-BR solution was 6 and was not adjusted during the photocatalytic oxidation tests.

Sulfuric acid, hydrochloric acid, ammonium ferrous sulfate, silver sulphate, mercury sulfate, silver nitrate, copper nitrate, butyl titanate, nitric acid, acetic acid, phenanthroline, cetyltrimethylammonium bromide (CTMAB), ethanol. The chemical reagents listed are analytically pure.

Pretreatment of expanded perlite (EP): Expanded perlites were prepared as the following steps: Expanded perlites were

screened *via* 8-10 mesh and washed to no dust. Then the samples were cleaned with deionized water to remove the ion from the sample. Rinsing was repeated 8-9 times. The final suspensions were dried the samples at 80 °C.

Preparation of HCEP: HCEP was prepared by adding a certain amount pretreatment expanded perlites into 4 mol/L sulfuric acid solution, stirring 2 h at 60 °C, after filtration they were dried under 105 °C for activation 2 h. The second step was adding the sulfuric acid modified expanded perlites into 5 % CTMAB solution, then were stirred for 2 h at 60 °C and filtration. The final suspensions were dried the samples at 80 °C for 2 h.

Preparation of TiO_2: It was prepared as follow steps: After 34 mL of butyl titanate solution adding into 136 mL of anhydrous ethanol solution, they were stirred strongly for 3 h to form flaxen butyl titanate/ethanol solution. And then 5.2 mL of glacial acetic acid was added for stirring 1 h and 72.8 mL of mixture solution of water and anhydrous ethanol (C_2H_5OH 65 mL, H_2O 2.8 mL and HNO_3 1 mL) were dropped, stirred slowly at 60 rpm speed for 2 h. At last, they were kept static at room temperature for 24 h.

Preparation of TiO_2 loaded catalyst: TiO_2 loaded catalyst was prepared by adding compound modified expanded perlites into TiO_2 sol, after stirring for 3 h and cleaning with deionized water for 7-8 times, they were dried at 110 °C. The final suspensions were placed in the muffle furnace at high temperature for 2 h (HCTEP) .

Analysis method: The surface morphology of samples was determined by scanning electron microscopy (SEM, Hitachi S4800, Netherlands PHILIPS Company). The accelerating voltage is 10 kV. And the phase of the catalysts was identified by X-ray diffractometer (XRD, Netherlands PHILIPS Company). The ultraviolet-visible spectrophotometer spectra of the Reactive brilliant blue X-BR dye solution samples at 1 h interval during photocatalytic oxidation was measured *via* a spectrophotometer (UV-2100, Beijing Rayleigh Analytical Instrument Factory). The absorbance was recorded at the wavelengths from 200 to 800 nm. On the other hand, the samples were dried completely by a rotary steaming system (RE201C, Shanghai Yao Yu equipment limited company) and then pressed as KBr pellets to acquire the FTIR spectra by an FTIR spectrometer (WQF-200, Beijing Rayleigh Analytical Instrument Corp. Ltd., China). The scan range of the wavenumber was set from 4000 to 400 cm^{-1}. The photocatalytic oxidation products of Reactive brilliant blue X-BR solution in this study were also identified by a GC-MS system (Agilent 5973N, Agilent Technologies co., LTD). Before analyzing with the GC-MS system, the products were extracted using ethyl acetate solvent in a separating funnel for three times.

Photocatalytic oxidation experiments [8]: The photocatalytic oxidation experiments were conducted at room temperature by a photocatalytic reactor. The reactor included ultraviolet lamps (160 W, main wave lenghth 253.7 nm) and magnetic stirrers which provided complete mixing of photocatalyst and X-BR solution. All experiments were explored with the following conditions: the amount of catalyst, the pH value, the calcination temperature, the concentration of X-BR solution and the loading time. The magnetic stirring time is 2 h.

RESULTS AND DISCUSSION

Catalyst preparation conditions

Influence of TiO_2 loading times for modified conditions: All experiments were performed under the same conditions (the dosage is 0.6 g, pH is 6 ± 0.1, the calcination temperature is 550 °C, the concentration of X-BR solution is 50 mg/L) but different loading times (1, 2, 3, 4, 5). The effect of the loading times of TiO_2 on removal rate was explored (Table-1).

TABLE-1
CHROMA AND THE COD REMOVAL PERCENTAGE UNDER VARIOUS LOAD TIMES

Loading times	1	2	3	4	5
Chroma removal rate (%)	88.15	91.51	94.25	94.02	94.05
COD removal rate (%)	78.81	79.84	82.59	82.51	82.51

It is indicated that the removal rate increased with the increace of the loading times. But when the loading time exceeded a critical value, 3 times, the removal rate did not increase any longer, which meant the oxidation function of photocatalyst could serve the reaction well at this moment when the COD and chroma removal rate reached 82.59 and 94.25 %, respectly. There are a lot of cavities on the surface of EP which make EP have large specific surface areas. The samples' specific surface area placed unevenly under lower loading times. With the increace of loading times, TiO_2 distributed more evenly, so increaced the samples' specific surface areas. However, too much capacity of TiO_2 would increase the sedimentation rate, therefore, reduced the efficiency of photocatalytic oxidation.

Influence of calcination temperature for modified conditions: All experiments were performed under the same conditions (loading 3 times) but different calcination temperatures (300, 400, 500, 550 and 600 °C).

As it is shown in Table-2, with the increase of the calcination temperatures, the COD and chroma removal rate gradually enhanced. When the calcination temperature reached 550 °C, the removal rate was best. However, higher temperature reduced the removal rate. This may because TiO_2 crystal type developed uncompletely under lower calcination temperatures. With the increace of calcination temperatures, TiO_2 crystal type changed from amorphous to anatase.

TABLE-2
CHROMA AND THE COD REMOVAL PERCENTAGE UNDER VARIOUS CALCINATION TEMPERATURE

Temperature (°C)	300	400	500	550	600
Chroma removal rate (%)	85.82	87.21	90.52	94.25	92.1
COD removal rate (%)	74.79	77.32	81.3	82.59	81.01

Photocatalytic activity measurements

Influence of pH for the chroma and COD removal rate: All experiments were performed under the same conditions but different pH values (2 ± 0.1, 4 ± 0.1, 6 ± 0.1, 8 ± 0.1, 10 ± 0.1, 12 ± 0.1). The influence of pH is shown in Fig. 1. When the pH value increased from 2 ± 0.1 to 6 ± 0.1, the COD removal rate increased from 72.31 to 82.59 %.

The results indicated that alkaline conditions conducive to the degradation of X-BR. The pH values can affect the stability of the dye molecules, the formation of free radicals and dispersivity, activity, surface charge of the photocatalyst, *etc*. The liquid diffusion rate of granular materials in the reaction changed with different pH values. Under high pH values, the light holes reacted with OH^- to generate hydroxyl free radical $^{\bullet}OH$ and then accelerate the degradation rate of X-BR in the alkaline condition. As Fig. 1, when pH is above 6 ± 0.1, the degradation rate of X-BR flat out.

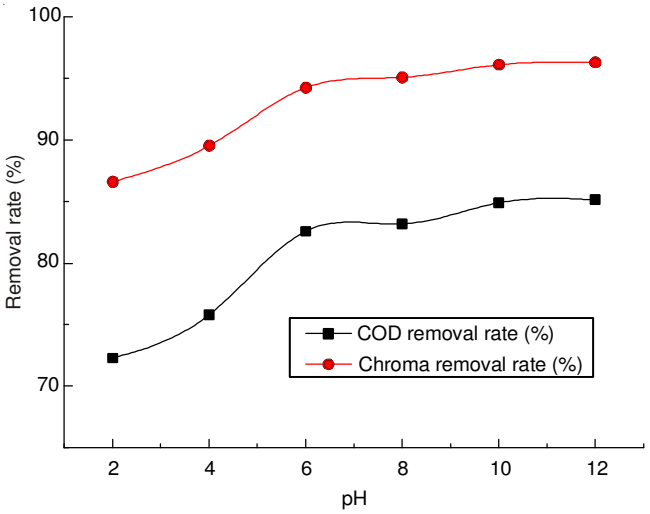

Fig.1. Effect of pH on removal rate of chroma and COD

Influence of dosage for the chroma and COD removal rate: All experiments were performed under the same conditions but different dosages (0.2, 0.4, 0.6, 0.8 and 1 g). The influence of dosage for the chroma and COD removal rate was explored (Fig. 2).

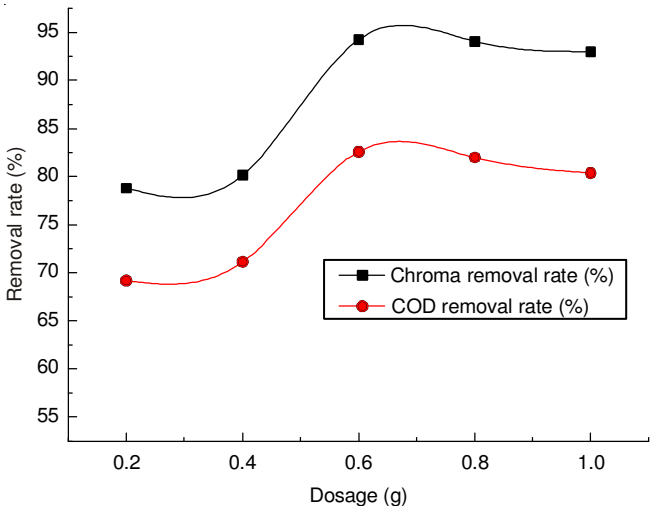

Fig. 2. Effect of dosage on removal rate of chroma and COD

When the dosage is lower than 20 g/L, the removal rate enhanced gradually with the increace of dosage. The removal rate enduced when the dosage was higher than 20 g/L. It can be explained that under lower dosage, the efficiency of effective photon converted into chemical energy was low and thus reduced the rate of reaction. On the other hand, particles would produce light shielding scatterings under higher dosage, reduced the solution transmittance.

Influence of dye concentration for the chroma and COD removal rate: All experiments were performed under the same conditions but different concentrations of X-BR solution (20, 50, 100, 200 and 500 mg/L).

Fig. 3 showed the result of the the influence of dye concentration for the COD and chroma removal rate. It is found that the COD and chroma removal rate deduced with the increase of the solution concentration. On the one hand, the higher of solution concentrations, the lower of solution transparency. Titanium dioxide can not be activated because of the light intensity of ultraviolet irradiation on the surface was abated, thus reduced the removal rate. On the other hand, photocatalyst has a certain amount of activated sites, the activity can't satisfy the need of high concentration at high solution concentration, results in the decrease of removal rate.

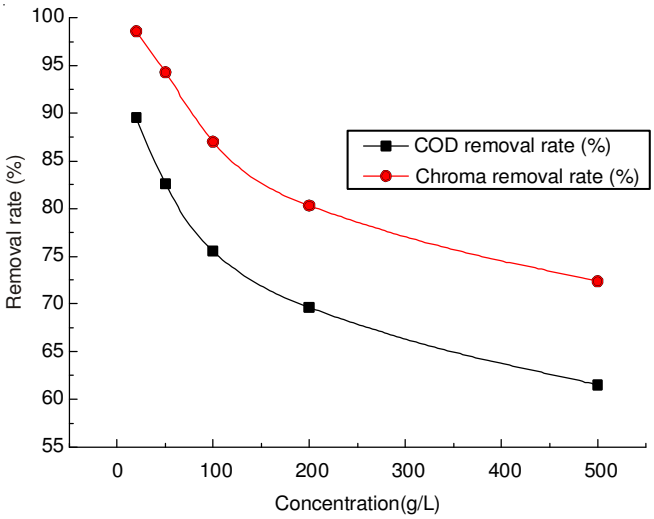

Fig. 3. Effect of concentration on removal rate of chroma and COD

Influence of reaction time for the chroma and COD removal rate: All experiments were performed under the same conditions but different reaction time (0.5, 1, 1.5, 2, 2.5 and 3 h). As seen in Fig. 4, the COD and chroma removal rate enhanced with the increase of the reaction time. After 2 h, the removal rate flattened out. In the process of chemical reaction, positive reaction almost simultaneous with adverse reaction, the reaction reached chemical equilibrium at 2 h, the change of chroma and COD removal rate is not obvious.

Mechanism aspects of photocatalytic of X-BR

SEM and XRD analysis: The SEM photos of TiO_2/EP composites which loaded three times, calcinated under 550 °C were displayed in Fig. 5. Expanded perlites have porous foam structures and on the surfaces covered with a mass of shallow pits. The pits had closed bottoms which make expanded perlite suitable as a floating photocatalyst carrier. Expanded perlites could not only float on the water for a long time, but could also provide active sites for nanometer TiO_2. As shown in Fig. 5 the TiO_2 particles had uniform loaded into the pores of expanded perlites which is consistent with the above experimental results.

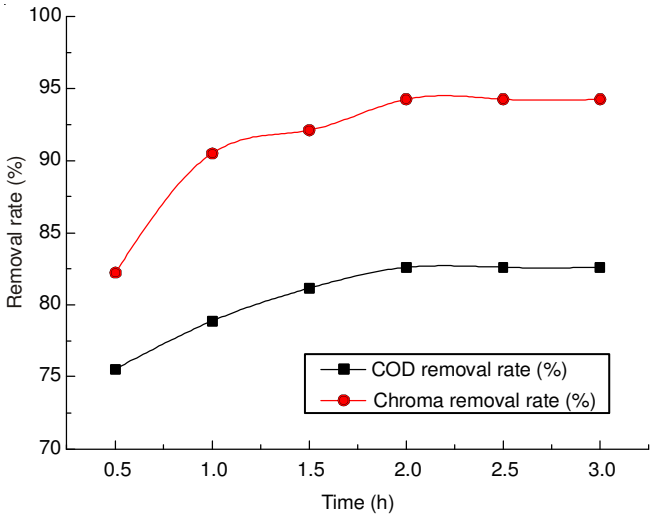

Fig. 4. Effect of shaking time on removal rate of chroma and COD

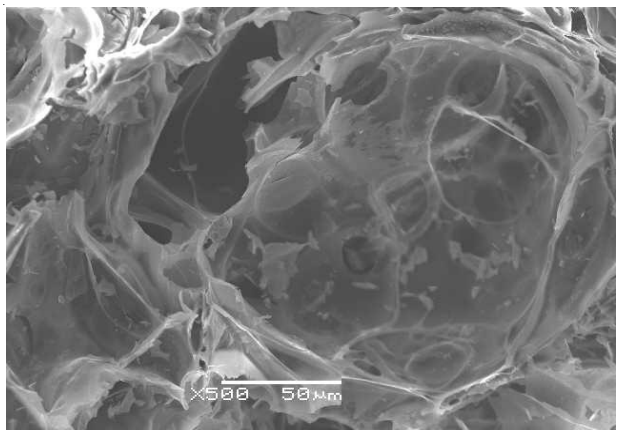

Fig. 5. SEM photo of microstructure of TiO_2/EP Composite materials

Fig. 6(a) to (f) represented the X-ray diffraction pattern of pure EP and EP with loaded times from 1 to 5, respectively. Little TiO_2 has entered into the porosity of EP under lower loaded times and no diffraction peak of TiO_2 has been found. With the increace of loaded times, the diffraction peaks of TiO_2 became clear. Anatase TiO_2 is obviously at 3 loaded times. Fig. 6 shows that the catalyst activated sites is short at lower loaded times, however, more than 3 loaded times, catalysts were more actively and could degrate the target objects directly on the catalyst activite sites, thus enhance the removal rate. But too much TiO_2 would plug the porosities of EP, reduced the catalyst activite sites, the specific surface areas and catalytic activity.

UV-visible scans analysis: The percentage of absorbance reduction of X-BR solution in the UV/visible spectra at different photocatalytic oxidation reaction time was shown in Fig. 7. There were four major characteristic absorption bands of X-BR: in the UV region of 256 nm characterizes the benzene ring structures, 290 nm characterizes the triazine structures, while 360 nm characterizes the double benzene nucleus structures. Other is in visible region of 596 nm characterizes the anthraquinone structures. The anthraquinone structures were the chromophore components of the dye molecules which could easily absorb ultraviolet light that produced electron transition and generated excited electrons. The excited electrons

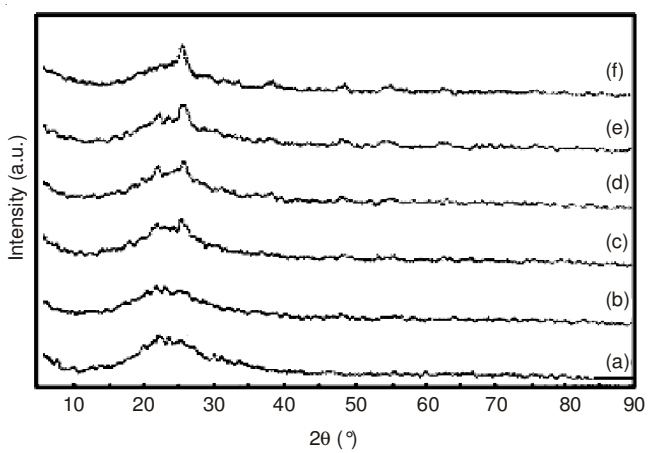

Fig. 6. XRD spectras of photocatalysts with different TiO_2 loading times

could activate the molecule's local structure which unstabled the carbon atoms linked to azo groups that cracked the N-C key first. The percentage of absorbance at 596 nm wavelengths gradually decreased with the increase of reaction time (Fig. 7). Thus it can be conclued that the anthraquinone structures were destroyed. At the same time, the characteristic absorption peaks between 200 and 400 nm were gradually reduced which indicated that the original molecules of the compound conjugated system were attacked by •OH and were gradually destroyed. This was just exactly in accord with the decolouration of X-BR solution. The results (Fig. 7) stated that the destruction of the conjugate structure was almost synchronized with the processing of decolourization. On the one hand, the destruction of the conjugated system melt the function of chromophore away. On the other hand, the loss of auxochrome groups also decolourized the X-BR solution. In other words, photocatalytic oxidation treatment was a gradual process which made it decolourization and degradation by changing the molecular structure of dye. So the mechanism was mainly through the rupture of unsaturated bond of the dye chromophores which broken by •OH directly, then be decomposed into small molecules.

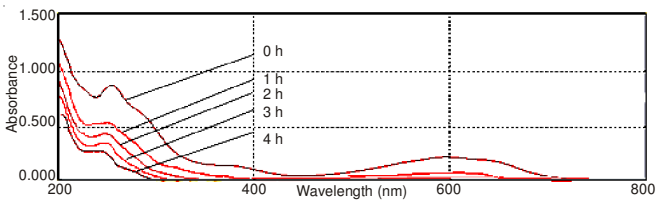

Fig. 7. UV-visible absorption spectra of Reactive Blue X-BR (t = 0-4 h) in photo-catalytic oxidation process

Infrared spectroscopic analysis: The transformation of the X-BR molecular structures were further evaluated by measurement of the FTIR spectra at 0 and 4 h. The results shown in Fig. 8a were the FTIR spectra of X-BR solution without photocatalytic oxidation and Fig. 8b was the FTIR spectra of X-BR solution after photocatalytic oxidation for 4 h. As the peaks of the wavenumber at 3050 ± 50 and 1650-1450 cm^{-1} belonged to C-H bond stretching vibration of aromatic ring and aromatic skeleton vibration, respectively. The peaks between 910 and 650 cm^{-1} were the bending vibration

peaks of aromatics C-H. The single substituted benzene presence of peaks observed between 710 and 690 cm^{-1}. As a results that the peaks of 3091, 1576 and 692 cm^{-1} shown in Fig. 8a were determined as the absorption peaks of benzene ring. The peak at 1335 cm^{-1} was the absorption peak of nitrogen atom C-N bond which linked to aromatic amine. The strong absorption peaks at 3469, 1633 and 1597 cm^{-1} were caused by -NH. The peak of 3469 cm^{-1} belonged to the OH stretching vibration peak. The peak 1194 cm^{-1} was the R-SO_3^- absorption peak. The peaks at 1576, 1532 and 1475 cm^{-1} standed for the benzene, naphthalene ring and triazine ring vibration absorption peaks, respectively. The peaks between 860 and 800 cm^{-1} are the CH side bending vibration absorption of hydrogen which linked to benzene rings. In the structure of X-BR exists conjugated structrue C=O and there was -NH_2 on the benzene ring which was the main chromophore of X-BR. The characteristic absorption peaks of C=O and -NH_2 were appeared at 1195-1040 and 1630 cm^{-1}, respectively, which correponding to the characteristic peaks at 1024 and 1633 cm^{-1} in Fig. 8a. The molecular structure of X-BR was in multiple of -C=C- functional groups, according of the infrared spectrograms, the weak but sharp absorption peak of 1576 cm^{-1} was the characteristic absorption peak of double bond of stretching vibration absorption. C-O-C groups of characteristic peaks were range from 1175 to 1038 cm^{-1}, thus it can be conclued that there were C-O-C groups in the structure of X-BR[9,10].

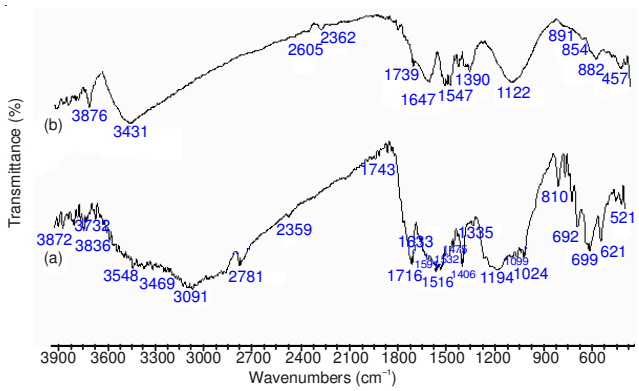

Fig. 8. IR spectra of pretreatment Reactive Blue X-BR in photo-catalytic oxidation process

New absorption peaks appeared at 3431 cm^{-1} which indicated the existence of functional groups containing hydrogen ion (-OH, -COOH, -NH, *etc*.) as shown in Fig. 8b. In general, the peaks of 3420-3250 cm^{-1} were the hydroxyl stretching vibration absorption peaks. Owing to the H on the aromatic ring was vulnerable by hydroxyl radicals and generated unstable hydroxyl replaced intermediates, thus there were hydroxyls in the reaction products. It can be infered that the wide peak at 3431 cm^{-1} was the hydroxyl absorption peak[11]. Furthermore, due to the strong oxidizing of hydroxyl free radicals, it can also be concluded that C has been oxidized to CO_2 or carbonate as the peaks at 1487 and 854 cm^{-1} are the absorption spectrum peaks of CO_3^{2-}.

The characteristic absorption peaks of 1670-1650 and 1320-1211 cm^{-1} were representative of C=O groups in carboxylic groups (-COOH) and C-O groups, respectively. From Fig. 8b we can see that the peak of 1647 cm^{-1} was strong and sharp and the peak of 1284 cm^{-1} was weak. It can be conclued that the peak of 1647 cm^{-1} was the absorption peak of C=O groups, the peak of 1284 cm^{-1} was the absorption of C-O groups, $V_{C=O}$ 1670-1650 cm^{-1} and V_{C-O} 1320-1211 cm^{-1} were the correlation peaks of carboxylic acid groups (-COOH). It can be refered that the products may containing carboxylic acid groups (-COOH). The characteristic peaks between 1090 and 990 cm^{-1} were due to presence of SO_4^{2-}, there were strong absorption peaks at 1049 and 1122 cm^{-1} which can conclude that the water containing SO_4^{2-} after handing and the reaction products still exist C-O-C groups. This is similar with Fenton oxidation degradation of X-BR[12].

GC-MS analysis: In order to verify the above deductions, a further attempt was made to identify the photocatalytic oxidation intermediate products of X-BR through GC-MS analyses. The qualitative results of the GC-MS analysis in Table-3 showed that some volatile intermediate products of X-BR solution were identified during photocatalytic oxidation.

TABLE-3
PHOTOCATALYTIC OXIDATION PRODUCTS OF X-BR IDENTIFIED BY GC-MS ANALYSIS

Number	Retention time (min)	Chemical formula
1	2.242	C_6H_6O
2	2.623	$C_4H_4O_4$
3	2.944	$C_2H_2O_4$
4	3.143	$C_6H_6NO_3S$
5	3.863	$C_3H_2N_4Cl_2$
6	7.776	$C_{10}H_6NO_5S$
7	17.869	$C_{16}H_{10}N_2O_8S_2$
8	18.499	$C_{19}H_{10}N_6O_8S_2Cl_2$

The *m/z* value of 95 belongs to the small molecular products. Speculated from the ion abundance ratios, it may be phenol which was the resultant of naphthalene and benzene oxidized by hydroxyl free radical, with the molecular formula being C_6H_6O (Fig. 9a). The molecular ion peak of *m/z* = 116 belongs to 2-butyl diacid generated by open-loop benzene, with the molecular formula being $C_4H_4O_4$ (Fig. 9b); the *m/z* value of 144.6 may belongs to adipic acid (Fig. 9c). The *m/z* value of 172 appeared the ion abundance ratios peaks of 9:6:1 as in Fig. 9e which indicated that there were two chlorine atoms; in the molecular structure of X-BR, the molecular mass of l, 3-dichloro-5-amino triazine group was at *m/z* = 173 which extrapolated that the *m/z* value of 172 may belongs to 1,3-dichloro-5-amino triazine. At the same time, the molecular ion peak of *m/z* 172 was further evidence that 1-amino-2-sulfonic acid sodium phenol triazines were broken into sulfamic acid and chlorinated triazine intermediates and the benzene rings were degradated. The *m/z* value of 170 (Fig. 9d) and 272 (Fig. 9f) were likely to be the degradation intermediates of naphthoquinone structures wihch attacked by hydroxyl radical ($^{\bullet}OH$), the molecular ion peak of *m/z* 170 belongs to sulfamic acid fragment peaks, with the molecular formula being $C_6H_6NSO_3$ which suggested that anthraquinone bonds were oxidized by $^{\bullet}OH$ to generate amino sulfonic acid, the formula of *m/z* = 272 was $C_{10}H_6NSO_5$. The molecular ion peak of *m/z* 422 belongs to naphthoquinone structure (Fig. 9) which was the resultant of X-BR lost triazine structure, with the molecular formula being $C_{16}H_{10}O_8N_2S_2$. The *m/z* value of 588 belongs to the

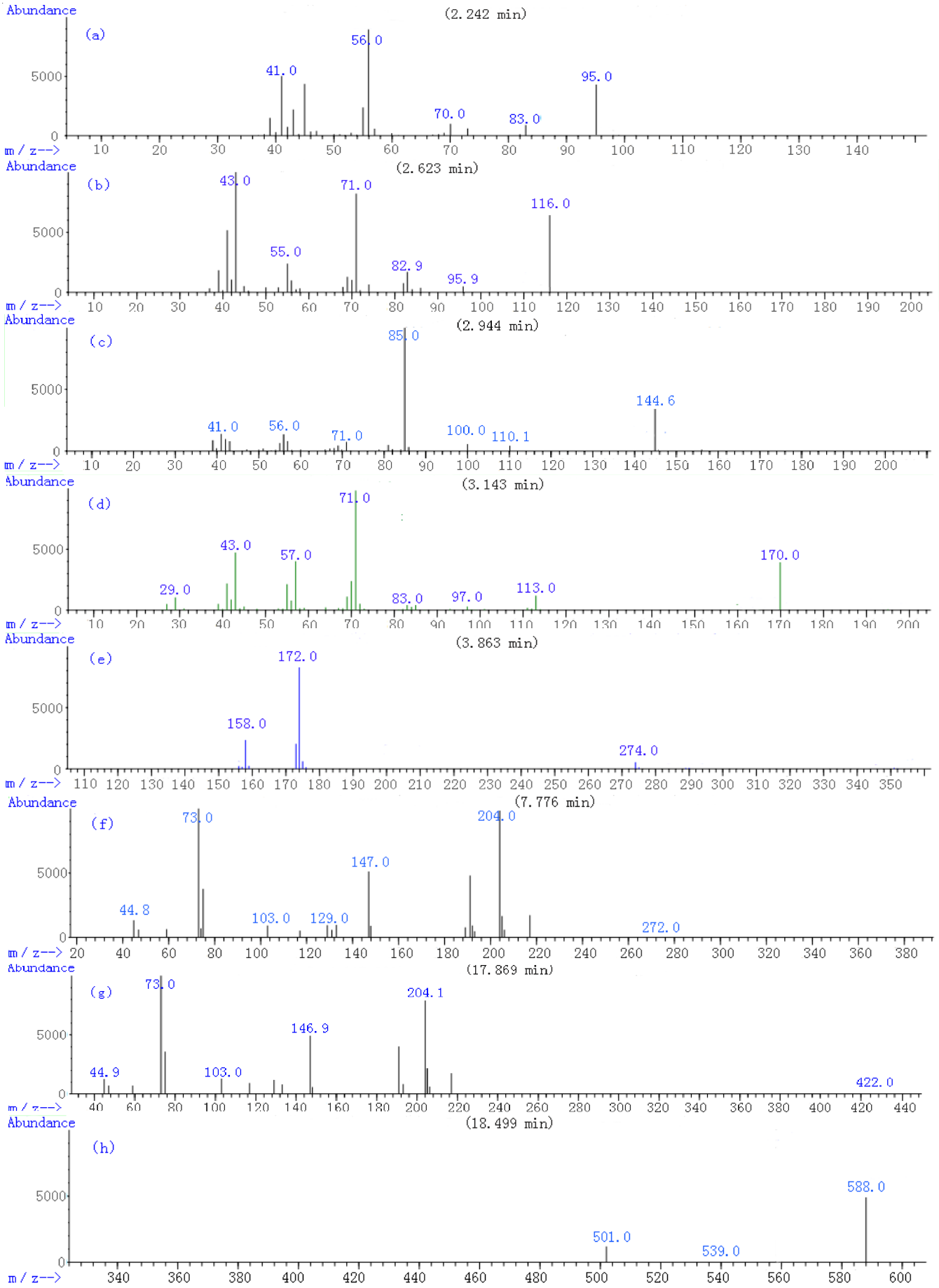

Fig. 9. GC-MS spectras of identified compounds in Reactive brilliant blue X-BR solution of photocatalytic oxidation

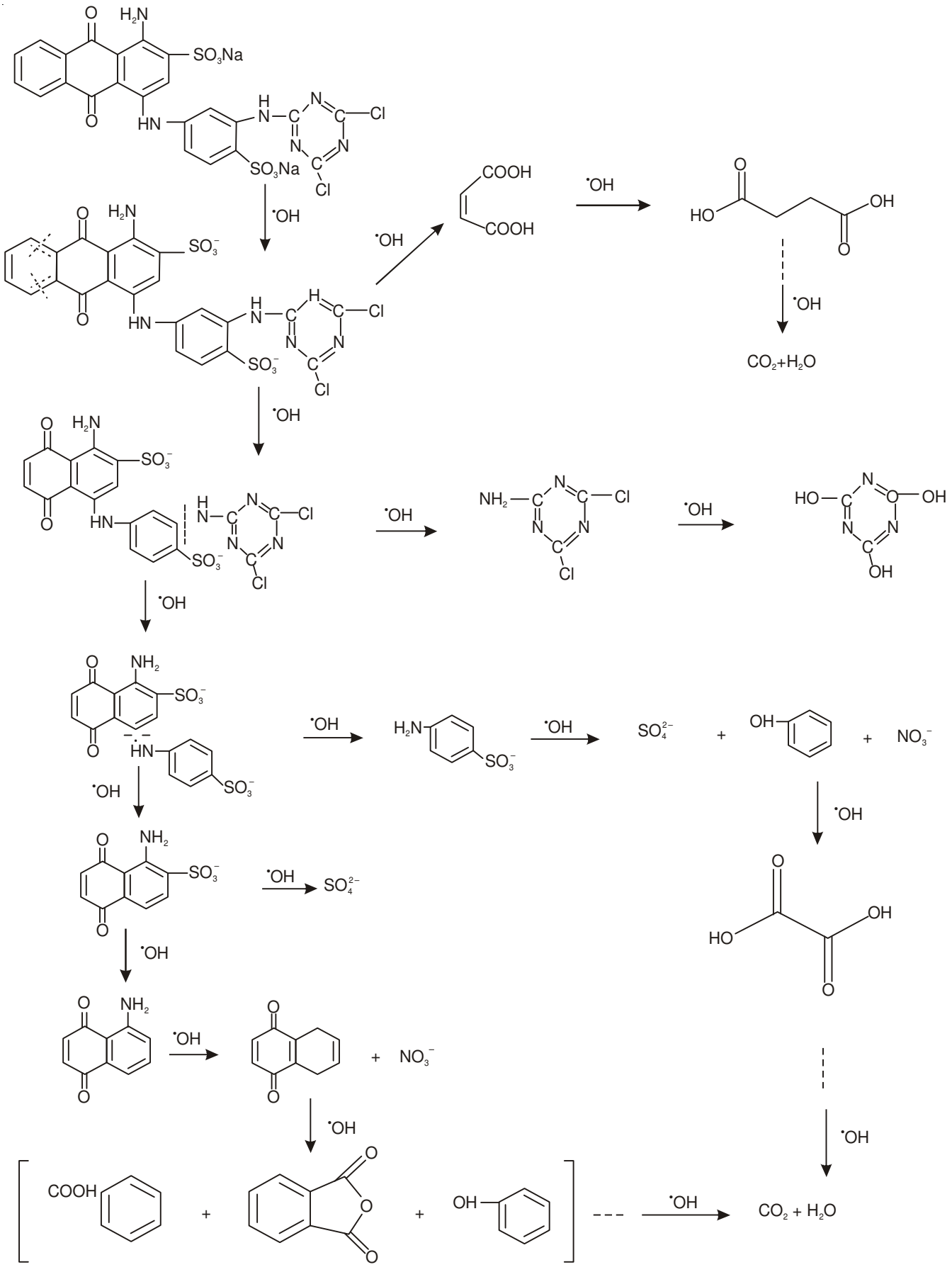

Fig. 10. Degradation pathways of Reactive brilliant blue X-BR reacting with photocatalytic oxidation

products after the benzene ring which on the left side of anthraquinone ring attacked by hydroxyl radical (•OH), its molecular formula was $C_{19}H_{10}N_6O_8S_2Cl_2$ (Fig. 9) and it was in line with the analysis results of UV and IR spectrograms[13].

Fig. 10 depicts the degradation pathways of X-BR[14-16]. based on the above analytical results. There are benzene rings, triazines, double benzene nucleus and anthraquinone structures in the molecules of X-BR. In the process of photocatalytic oxidation treatment of X-BR, hydroxyl radicals firstly attacked the benzene ring on the left side of anthraquinone ring. The reason of which is that the electron cloud density of anthraquinone ring was higher than the other side and also the ring had been degraded to 1-amino-2-sulfonic acid sodium phenol triazine and 2-ene succinic acid. Then the 2-ene succinic acid lost an electron which captured by ·OH and formed succinic acid. The succinic acid continued to be degraded to CO_2 and H_2O through a series of reactions. And then 1-amino-2-sulfonic acid sodium phenol triazine continued to be broken into amino sulfonic acid and chlorinated triazine intermediates. Finally, hydroxyl radicals directly attacked H ion on the naphthalene ring, which generated phenol that was degraded into small molecule acid and water at last and -SO_3Na falled off which was oxidized to inorganic ion SO_4^{2-} after the reaction of hydroxyl substitution.

Conclusions

(1) The crystalline titanium dioxide prepared by sol-gel method is anatase which has a good performance of photocatalytic oxidation, loaded on the expanded perlite can be a kind of efficient adsorption catalyst which can float on the surface of water and easy to be recycled.

(2) Analyse from the variety of spectra and chromatograms, the results of the present work showed that the degradation of X-BR in aqueous solution by photocatalysis oxidation is that hydroxyl radicals firstly attacked the chromophore which arounded the anthraquinone ring and made it destruction and decolourization; then the groups such as naphthoquinone, benzene, *etc.* which were easily to be oxidized were attacked. Finally, the triazine structure degraded. The degradation of intermediates mineralized into inorganic substances ultimately after a series of process.

REFERENCES

1. J.M. Fanchian and D.H. Tseng, *Chemosphere*, **77**, 214 (2009).
2. L. Qi, J. Yu and M. Jaroniec, *Adsorption*, **19**, 557 (2013).
3. H. Zhang, R. Zong, J. Zhao and Y. Zhu, *Environ. Sci. Technol.*, **42**, 3803 (2008).
4. I. Rosenberg, J.R. Brock and A. Heller, *Physical Chem.*, **96**, 8 (1992).
5. H. Liao, X.L. Xu, W.Q. Chen, Q.-J. Shi, W.-M. Liu and X. Wang, *Acta Phys.-Chim. Sin.*, **28**, 2924 (2012).
6. X. Lv, T.J. Peng, H.J. Sun and C.J. Gu, *J. Synth. Cryst.*, **42**, 290 (2013).
7. W.B. Zou, *Sichuan Cement*, **05**, 15 (2008).
8. Q.Q. Gao, The Research of Preparation of Different Modified Expanded Perlite and Removal of Organic Pollutants in Environmental, Yangzhou University, Yangzhou, Jiangsu, China (2010).
9. Y.P. Du, Modern Instrumental Analysis Methods, East China University of Science and Technology Press; Shanghai, China (2008).
10. M.H. Habibi and M.K. Sardashti, *Adv. Oxid. Technol.*, **12**, 231 (2009).
11. S.K. Kansal, A.H. Ali, S. Kapoor and D.W. Bahnemann, *Sci. Adv. Mater.*, **5**, 630 (2013).
12. X.Q. Wang, X.M. Hu, Y.Q. Ma, *Environ. Prot. Chem. Ind.*, **6**, 482 (2010).
13. H. Zhang, Q.J. Peng and Y.M. Li, *Chem. Ind. Press*, **27**, 377 (2005).
14. Y.J. Li, J.S. Wang, L. Tian and Q.L. Zhu, *J. Lanzhou Jiaotong Univ.*, 84 (2005).
15. J. Dong and C.A. Migdal, in ed.: L.R. Rudnick, Lubricant Additives Chemistry and Applications, CRC Press pp. 3-29 (2009).
16. Y.P. Mao, Y. Tao, Z.-M. Shen, Y.-M. Lei and W.H. Wang, *Environ. Sci. Technol.*, **32**, 67 (2009).